Analytical Methods

ROYAL SOCIETY OF CHEMISTRY

PAPER

View Article Online
View Journal | View Issue

Cite this: *Anal. Methods*, 2025, **17**, 2536

Development of a novel label-free NIR aptasensor based on triphenylmethane dyes for rapid and sensitive detection of copper ions†

Junhao Hu,[a] Xinxin Li,[a] Teck-Peng Loh *[ab] and Lingli Bu *[a]

Received 29th January 2025
Accepted 24th February 2025

DOI: 10.1039/d5ay00156k

rsc.li/methods

Heavy metal pollution, particularly from copper ions (Cu^{2+}), poses a significant threat to both the ecological environment and human health. However, traditional copper ion analysis techniques are often hindered by the need for expensive equipment, labor-intensive sample preparation and skilled operation, which limits their effectiveness for field and real-time applications. In this work, we report a novel near-infrared aptamer sensor (NIRApt) that originates from the binding reaction between the DNA aptamer Apt_{Cu} and the fluorescent small molecule crystal violet (CV), enabling rapid detection of Cu^{2+} through the competitive effect of Cu^{2+} with Apt_{Cu}. This sensor shows a significant enhancement in NIR fluorescence after aptamer binding. NIRApt exhibits superior performance, requiring only three core components to achieve a fast response time and operational simplicity in less than a minute. The sensor shows high sensitivity with a detection limit as low as 61 nM, making it suitable for the detection of trace amounts of Cu^{2+} in diverse samples. The efficacy of NIRApt has been validated through successful applications in real water samples, highlighting its promising potential for environmental monitoring.

1. Introduction

Heavy metal pollution, particularly Cu^{2+} contamination from industrial activities such as mining, electroplating and electronics manufacturing, poses severe threats to both the environment and human health. As a persistent and bioaccumulative pollutant, Cu^{2+} exhibits chronic toxicity in aquatic ecosystems.[1,2] Prolonged exposure to elevated Cu^{2+} levels can severely damage vital organs, such as the cerebrum, kidneys and gastrointestinal system.[3–5] Regulatory agencies, including the European Commission and the US Environmental Protection Agency, have set stringent thresholds for Cu^{2+} concentrations in drinking water, at 2 mg L^{-1} and 1.3 mg L^{-1}, respectively.[6,7] The urgent need for precise and portable detection methods is underscored by the necessity to mitigate Cu^{2+} contamination in environmental and food samples.

Conventional analytical techniques, such as atomic absorption spectroscopy, inductively coupled plasma mass spectrometry and atomic emission spectroscopy, deliver high sensitivity and reliability.[8–11] However, these methods are hampered by their dependence on expensive equipment, labor-intensive sample preparation and skilled operation. Such limitations significantly hinder their application for on-site and real-time monitoring. Fluorescence-based detection strategies, in contrast, offer distinctive features, including high specificity and sensitivity, real-time monitoring, operational simplicity and cost-effectiveness, making them highly suitable for practical applications across various fields.[12–15]

Among fluorescence-based technologies, nucleic acid-based sensing platforms, especially those utilizing aptamer recognition elements, have emerged as particularly promising candidates. Aptamers are short oligonucleotide sequences capable of binding specific targets, such as ions, small molecules or proteins, with unparalleled specificity and binding affinity.[16–18] Although significant progress has been made in aptamer-based Cu^{2+} detection systems, current designs predominantly depend on visible-range fluorescence detection, making them susceptible to interference from complex sample matrices.[19,20] Near-infrared (NIR) fluorescence has emerged as a promising solution for environmental detection, offering minimized background interference and enhanced detection accuracy.[21–23] These unique spectral properties make NIR particularly suitable for *in situ* and real-time monitoring applications.

Triphenylmethane (TPM) dyes, as one of the earliest synthetic dye classes, possess unique characteristics including nucleic acid binding affinity, intrinsic NIR fluorescence, excellent photostability and water solubility. These properties, coupled with their small molecular size and cost-effectiveness, have facilitated their widespread application in biosensing and

[a]*Henan Linker Technology Key Laboratory, College of Advanced Interdisciplinary Science and Technology (CAIST), Henan University of Technology, Zhengzhou 450001, China. E-mail: linglibu@163.com*

[b]*Division of Chemistry and Biological Chemistry, School of Physical and Mathematical Sciences, Nanyang Technological University, Singapore 637371, Singapore. E-mail: teckpeng@ntu.edu.sg*

† Electronic supplementary information (ESI) available. See DOI: https://doi.org/10.1039/d5ay00156k

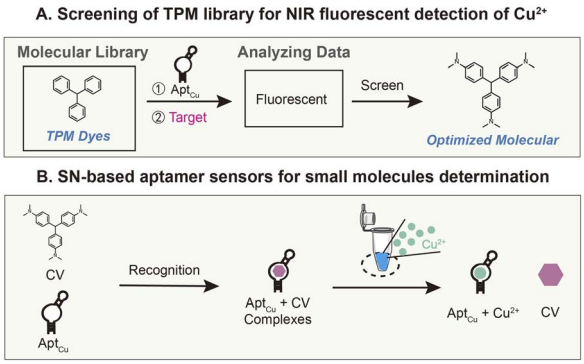

Scheme 1 (A) Schematic diagram of TPM dye screening for the NIR aptasensor and (B) the construction of the NIR aptasensor for Cu^{2+} detection.

bioimaging.[24] The strategic integration of TPM dyes with an aptamer-based platform presents a promising strategy for developing highly sensitive and specific detection systems.

Herein, we present a novel near-infrared aptasensor (NIRApt) platform utilizing TPM dyes for highly selective and sensitive Cu^{2+} detection (Scheme 1). Through systematic construction and evaluation of an extensive TPM molecular library in combination with a Cu^{2+}-specific aptamer, we identified an optimal dye–aptamer pair demonstrating a remarkable NIR fluorescence change upon target recognition. The developed NIRApt exhibits outstanding performance, featuring an ultra-fast response (<1 min) and simplified operation through its three-component design. The sensor achieved high sensitivity with a low detection limit, enabling reliable quantification of trace Cu^{2+} in diverse samples. Furthermore, the practical utility of this sensing platform was successfully validated through its successful application in real water samples, demonstrating its promising potential for real-world environmental monitoring applications.

2. Experimental section

2.1. Materials and instruments

All the chemical reagents and instruments are presented in the ESI.†

2.2. Fluorescence spectroscopy

DNA oligomers were annealed in ultrapure water by heating at 95 °C for 10 min, and then slowly cooled to room temperature. Samples were measured by the addition of pre-prepared CV (100 μM) and annealed Apt_{Cu} (100 μM), followed by adding buffer to a final volume of 200 μL and then incubating for 5 min. Assays were conducted in a supporting electrolyte containing 10 mM MES, 100 mM NaCl, and 2 mM $MgCl_2$ (pH 6.0). To measure the binding constant of CV to Apt_{Cu}, different concentrations of Apt_{Cu} (0–10 μM) were mixed with 10 μL of CV (100 μM) in the reaction buffer. Sensitivity detection of Cu^{2+} using NIRApt sensors: different concentrations of $CuCl_2$ (0–30 μM) were added into the reaction buffer containing Apt_{Cu} (100 μM) and 10 μL of CV (100 μM) to record their fluorescence spectra. All experiments were conducted with excitation at 540 nm and a maximum emission wavelength of 640 nm was recorded. The multimode microplate reader measures fluorescence intensity values of 540–800 nm using a 384-well black microplate with an excitation and emission slit width of 20 nm. The formula for calculating the dissociation constant (K_d) from the unit-point specific binding model is as follows:[25]

$$Y = Y_{max} \times X/(K_d + X)$$

where Y represents the fluorescence fold change of the DNA oligomer; Y_{max} is the maximum fold change in fluorescence of the dye (CV) and X is the concentration of the DNA oligomer.

2.3. UV-vis analysis

First, 10 μL of CV (100 μM) and different concentrations of Apt_{Cu} (0–10 μM) were mixed in the reaction buffer and their UV absorption spectra were measured. Different concentrations of $CuCl_2$ (0–50 μM) were added to the mixture, containing 8 μL of Apt_{Cu} (100 μM) and 10 μL of CV (100 μM). UV-vis absorption spectra were recorded from 400 to 750 nm using a Spar multi-mode microplate reader.

2.4. Fluorescence quantum yield measurement

In this work, the fluorescence quantum yield (Φ) of the sensor was measured with Cy5 (PBS as solvent) as a standard (Φ: 27%) using the following equation:[26]

$$\Phi_x = \Phi_s \times \frac{I_x}{I_s} \times \frac{A_s}{A_x} \times \left(\frac{\eta_x}{\eta_s}\right)^2$$

where, Φ is the quantum yield, I stands for the integrated emission intensity, A is the absorbance, and η is the refractive index of the solvent. "s" refers to the standard with a known Φ and "x" refers to the sample. Absorption was kept below 0.05 at the excitation wavelength.

2.5. Real sample analysis

The lake water samples were collected from Henan University of Technology and $CuCl_2$ was added to prepare the samples to be tested with different concentrations of Cu^{2+}. To prepare the working solution for the detection of lake water samples, 10 μL of CV (100 μM) and 8 μL of Apt_{Cu} (100 μM) were added; different concentrations of the samples to be measured were added to the working solution, and MES buffer (pH = 6.0) was added as the supporting electrolyte, and the buffer was added to adjust the final volume of the system to 200 μL.

3. Results and discussion

3.1. Screening of the TPM library for NIR fluorescence-based detection of Cu^{2+}

The aptamer CU-1 (Apt_{Cu}), identified by Liu's group, was selected as the key sensing component for this study.[27] To complement this aptamer, a library of six TPM dyes was constructed (Fig. 1A and B). Each dye featured positive charges and distinct substituents on the benzene ring, enabling the

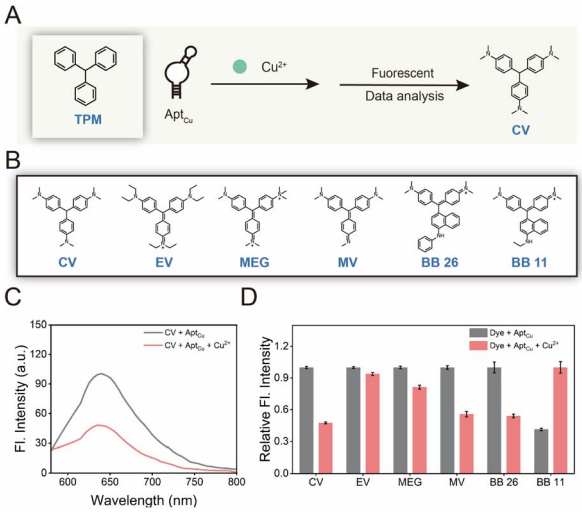

Fig. 1 (A) Screening of fluorescent dyes from the TPM dye library for their ability to bind to the aptamer and Cu^{2+}. (B) Chemical formulae of six selected TPM dyes. (C) Fluorescence spectra of CV dye in the presence or absence of Cu^{2+} in solution. (D) Relative fluorescence of the TPM dyes/Apt_{Cu} with or without Cu^{2+}.

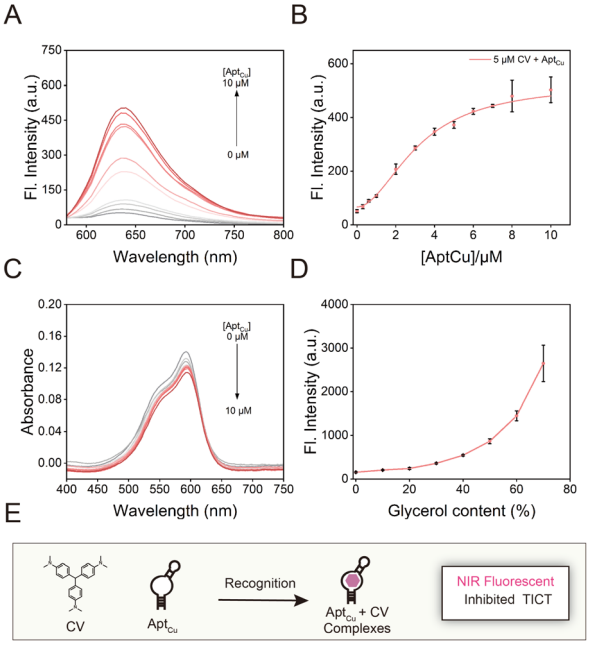

Fig. 2 (A) Fluorescence spectra of CV with different concentrations of Apt_{Cu} (0–10 μM), λ_{ex} = 540 nm. (B) Corresponding fluorescence intensity of CV combined with different concentrations of Apt_{Cu} at 640 nm. (C) CV absorption spectra with varying Apt_{Cu} concentrations. (D) Fluorescence intensity of CV in a mixture of MES buffer and glycerol. (E) Mechanism of fluorescence intensity change due to CV and Apt_{Cu} binding.

exploration of structural variations on fluorescence behavior and compatibility with the aptamer.

Screening experiments were performed by incubating each TPM dye (4 μM) with Apt_{Cu} (2 μM) in the presence and absence of Cu^{2+} (4 μM). All six TPM dyes exhibited significant fluorescence enhancement upon binding with Apt_{Cu}, confirming their strong interaction and potential as fluorophores in NIRApt (Fig. 1C and S1–S5†). The fluorescence emission was concentrated in the NIR region, highlighting the dyes' suitability for applications requiring minimal interference from complex samples. Upon the addition of Cu^{2+}, the fluorescence intensity decreased to varying degrees, demonstrating effective quenching behavior.

Among the dyes tested, crystal violet (CV) displayed the most pronounced fluorescence response, with a quenching ratio of 2.5-fold compared to the baseline (Fig. 1D). This robust response positions CV as the optimal candidate for sensor integration. Its favorable structural features likely contribute to enhanced interactions with Apt_{Cu} and heightened sensitivity to Cu^{2+}.

3.2. Interaction of TPM and Apt_{Cu} and their photophysical properties

To delve deeper into the high signal-to-noise ratio exhibited by the CV-based NIRApt sensor in Cu^{2+} detection, we investigated the underlying molecular mechanisms in detail. Our initial experiments assessed the binding affinity between CV and Apt_{Cu}. Fluorescence analysis revealed that CV alone exhibited negligible emissions in buffer. Upon the introduction of Apt_{Cu}, a marked enhancement in NIR fluorescence of CV was observed, peaking at an emission wavelength of 640 nm, and K_d for the formation of the Apt_{Cu}/Cu^{2+} complex was determined to be 2.44 μM (Fig. 2A and B). In parallel, UV-vis absorption spectra showed a slight decrease in the absorbance of CV after Apt_{Cu} binding, indicative of robust interactions (Fig. 2C).

To gain deeper insights into the mechanism responsible for the fluorescence enhancement, we evaluated the behavior of CV under varying viscosity conditions. Results showed a proportional increase in fluorescence intensity with increasing viscosity, consistent with restricted intramolecular rotations (Fig. 2D). This observation supports the hypothesis that Apt_{Cu} binding constrains the rotational freedom of the benzene ring within CV around its single bond, thereby suppressing the twisted intramolecular charge transfer state and enhancing fluorescence.[28,29] Collectively, these findings highlight that the interaction between CV and Apt_{Cu} not only induces significant changes in absorption but also effectively limits molecular motion, resulting in pronounced fluorescence enhancement (Fig. 2E).

3.3. CV-based NIRApt aptasensor for Cu^{2+} detection

The sensitivity of the CV-based NIRApt aptasensor is a critical factor influenced by the aptamer-to-dye concentration ratio. Here, we systematically evaluated how the Apt_{Cu} and CV concentration ratios impact the performance of the sensor. When the Apt_{Cu} : CV ratio was set to 0.8 : 1, a linear relationship was observed between the change in fluorescence intensity and Cu^{2+} concentration in the range of 0–2 μM, resulting in a limit of detection (LOD, 3σ) of 61 nM. When the ratio was adjusted to 1.4 : 1, the LOD slightly decreased to 67 nM (Fig. S6†). Furthermore, the Benesai–Hildebrand plots,[30] constructed from fluorescence titration curves for 4 and 7 μM Apt_{Cu}, confirmed

the 1 : 1 stoichiometric interaction between NIRApt with Cu^{2+}, yielding binding constant values of 7.52×10^5 M^{-1} and 3.47×10^5 M^{-1}, respectively (Fig. S7†). The optimized aptamer concentration of 4 μM significantly enhanced sensitivity (Fig. 3A–C), highlighting the critical role of the aptamer-to-dye ratio in determining NIRApt performance. CV dye exhibited a fluorescence quantum yield (Φ) of 0.08%, which increased to 1.24% upon Apt_{Cu} binding and decreased to 0.23% following Cu^{2+} addition. In conjunction with the changes observed in UV-vis absorption spectra (Fig. 3D and E), these findings further suggest the competitive interaction between Cu^{2+} and Apt_{Cu}.

To validate the selectivity of NIRApt, we tested its response to a broad array of common cations and anions typically found in aquatic environments, including Ca^{2+}, Zr^{4+}, Cr^{3+}, Cd^{2+}, Co^{2+}, Pb^{2+}, Fe^{3+}, Fe^{2+}, Na^{+}, Ni^{2+}, K^{+}, Mn^{2+}, Zn^{2+}, Hg^{2+}, Cu^{+}, HPO_4^{2-}, $H_2PO_4^{-}$, SO_4^{2-} and NO_3^{-}. No significant fluorescence was observed for any of the above ions, confirming the exceptional selectivity of NIRApt for Cu^{2+} (Fig. 3F). These results demonstrate that NIRApt enables highly specific Cu^{2+} detection, attributed to the strong binding affinity between Apt_{Cu} and Cu^{2+}, which surpasses that of other ions.

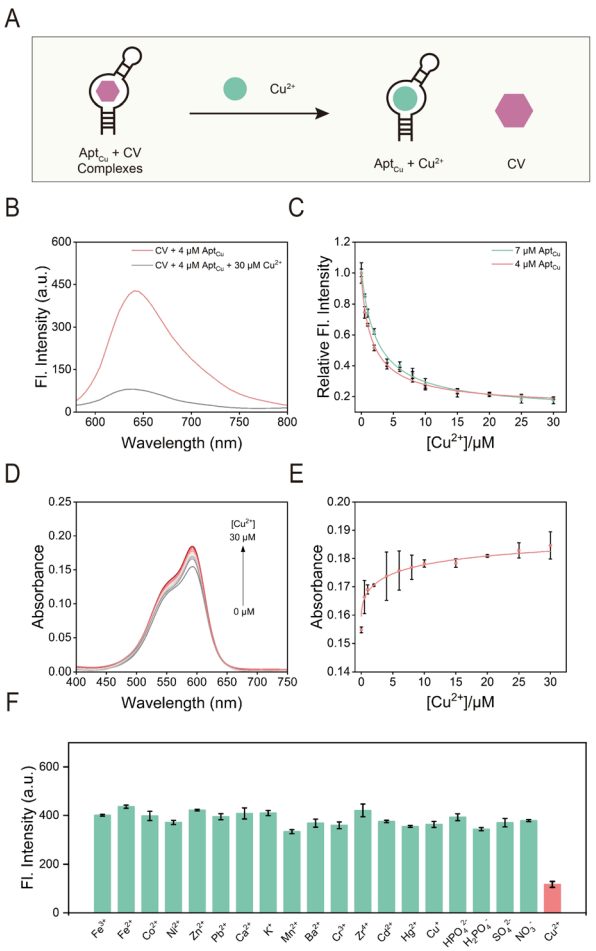

Fig. 3 (A) Cu^{2+} can displace CV dyes from NIRApt. (B) Fluorescence spectra of NIRApt with or without Cu^{2+}. (C) NIRApt was added to 4 or 7 μM Apt_{Cu} with different concentrations of Cu^{2+} at $\lambda_{em} = 640$ nm. (D) Absorption spectra of different concentrations of Cu^{2+} added to NIRApt. (E) The absorbance of different concentrations of Cu^{2+} in NIRApt. (F) Selectivity of NIRApt sensors for various ions.

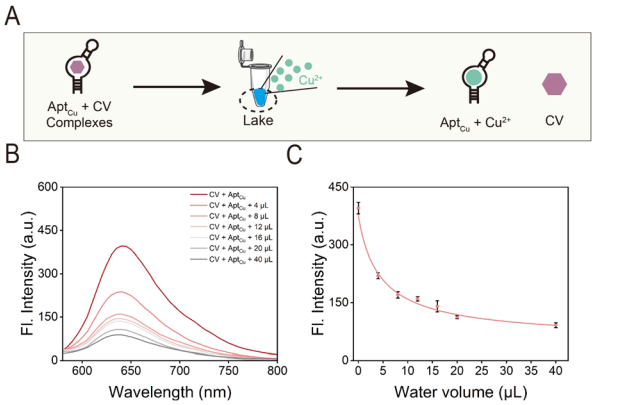

Fig. 4 (A) Schematic diagram of NIRApt-based Cu^{2+} detection in raw lake water. (B) Fluorescence emission spectra of NIRApt in the presence of varying volumes of lake water. (C) Fluorescence intensity of NIRApt when mixed with different volumes of ultrapure water or lake water samples.

Table 1 Determination of Cu^{2+} in lake water

Sample	Added (μM)	Found (μM)	Recovery (%)
Lake water	4	4.2342 (±0.18)	105.85
	6	6.0961 (±0.21)	101.60
	8	7.9879 (±0.35)	99.84
	10	10.2402 (±0.31)	102.40
	20	21.2312 (±0.82)	106.16

3.4. Practical application of NIRApt for Cu^{2+} detection

The rapid industrialization and growing anthropogenic impacts on aquatic ecosystems, particularly from sewage discharge, have heightened the need for effective environmental monitoring. Motivated by the excellent performance of NIRApt, we sought to explore its potential for sensitive Cu^{2+} detection in real water samples, aiming to develop advanced monitoring solutions. The results in Fig. 4A and B show a concentration-dependent fluorescence quenching at 640 nm, confirming Cu^{2+}-specific detection through fluorescence quenching. Six replicate measurements demonstrated consistent quenching responses, highlighting NIRApt's reliability in complex water samples. NIRApt demonstrated a Cu^{2+} detection range of 4–20 μM in real water samples, with recovery rates of 99.84–106.16% (Fig. 4C and Table 1). The results demonstrate the exceptional performance of NIRApt as a detection platform for Cu^{2+} in real water samples. Given the promising performance of NIRApt, we foresee its broader applications in detecting Cu^{2+} across diverse environmental samples, offering a versatile and highly sensitive tool for Cu^{2+}-related environmental research.

4. Conclusions

In summary, we developed a novel label-free near-infrared fluorescent aptasensor (NIRApt) that integrates TPM dyes with

a Cu^{2+}-binding aptamer (Apt_{Cu}) for Cu^{2+} detection. By optimizing the TPM dyes, we successfully developed a sensor that integrates CV and Apt_{Cu}, demonstrating highly selective and sensitive Cu^{2+} detection. This sensor offers excellent specificity, rapid response and a low detection limit of 61 nM. Moreover, we demonstrated that NIRApt is highly selective for Cu^{2+} over other relevant ions. Beyond its superior analytical performance, NIRApt offers practical advantages such as simple operation, rapid response, and strong anti-interference capabilities. These features make NIRApt highly suitable for detecting Cu^{2+} in real-world water samples, underlining its applicability for both laboratory and practical analyses. We expect that this approach will establish a new paradigm in Cu^{2+}-responsive sensor design, with considerable potential to improve environmental and water pollution monitoring.

Data availability

The data supporting this article have been included as part of the ESI.†

Author contributions

Junhao Hu: conceptualization, methodology, investigation, formal analysis and writing – original draft. Xinxin Li: methodology, formal analysis and writing – original draft. Teck-Peng Loh: supervision, conceptualization, funding acquisition, writing – review & editing. Lingli Bu: supervision, conceptualization, funding acquisition, writing – review & editing.

Conflicts of interest

The authors declare no competing financial interest.

Acknowledgements

We gratefully acknowledge the grants from the Key Technologies R & D Program of Henan Province (242102311229), Natural Science Foundation of Henan Province (242300421618) and Start-up Grant of Henan University of Technology (2022BS046, 2022BS047 and 2022BS053). We also gratefully acknowledge the financial support from the Distinguished University Professor grant (Nanyang Technological University) and the Agency for Science, Technology, and Research (A*STAR) under the MTC Individual Research Grant (M21K2c0114) and the RIE2025 MTC Programmatic Fund (M22K9b0049) for T.-P. L.

Notes and references

1 W.-W. Zhao, J.-J. Xu and H.-Y. Chen, *Analyst*, 2016, **141**, 4262–4271.
2 Y. Acar, B. B. Kandemir and A. T. Bayraç, *Talanta Open*, 2022, **6**, 100159.
3 A. A. Taylor, J. S. Tsuji, M. R. Garry, M. E. McArdle, W. L. Goodfellow, W. J. Adams and C. A. Menzie, *J. Environ. Manage.*, 2019, **65**, 131–159.
4 Z. Zhou, S. Chen, Y. Huang, B. Gu, J. Li, C. Wu, P. Yin, Y. Zhang and H. Li, *Biosens. Bioelectron.*, 2022, **198**, 113858.
5 A. K. Sharma, Priya, B. S. Kaith, A. Singh, Isha, Vipula and K. Chandel, *Chem. Eng. J.*, 2020, **382**, 122965.
6 R. Wang, Y. Cao, H. Qu, Y. Wang and L. Zheng, *Talanta*, 2022, **237**, 122965.
7 H. Gomaa, M. A. Shenashen, A. Elbaz, H. Yamaguchi, M. Abdelmottaleb and S. A. El-Safty, *J. Hazard. Mater.*, 2021, **406**, 124314.
8 D. Alexander, R. Ellerby, A. Hernandez, F. Wu and D. Amarasiriwardena, *Microchem. J.*, 2017, **135**, 129–139.
9 A. P. S. Gonzáles, M. A. Firmino, C. S. Nomura, F. R. P. Rocha, P. V. Oliveira and I. Gaubeur, *Anal. Chim. Acta*, 2009, **636**, 198–204.
10 I. D. la Calle, P. Pérez-Rodríguez, D. Soto-Gómez and J. E. López-Periago, *Microchem. J.*, 2017, **133**, 293–301.
11 Y. Liu, P. Liang and L. Guo, *Talanta*, 2005, **68**, 25–30.
12 H. Li, W. Shi, X. Li, Y. Hu, Y. Fang and H. Ma, *J. Am. Chem. Soc.*, 2019, **141**, 18301–18307.
13 M. Z. Alam and S. A. Khan, *J. Fluoresc.*, 2024, 1–16.
14 C. Hussain, A. Petrillo and S. U. Islam, *Concepts in Smart Societies: Next-Generation Of Human Resources And Technologies*, CRC Press, 2023.
15 M. Mohasin, M. Z. Alam, S. Ahmad, U. Salma, Y. Kumar, R. Patel, Q. Ullah and S. A. Khan, *J. Fluoresc.*, 2024, 1–10.
16 A. L. Chang, M. McKeague, J. C. Liang and C. D. Smolke, *Anal. Chem.*, 2014, **86**, 3273–3278.
17 S. Qian, D. Chang, S. He and Y. Li, *Anal. Chim. Acta*, 2022, **1196**, 339511.
18 W. Zhou, R. Saran and J. Liu, *Chem. Rev.*, 2017, **117**, 8272–8325.
19 Y. Mou, Y. Zhang, X. Lin, M. Chen, Y. Xia, S. Zhu, C. Wei and X. Luo, *Anal. Methods*, 2023, **15**, 3466–3475.
20 J. Wang, Y. A. Kaiyum, X. Li, H. Lei, P. E. Johnson and J. Liu, *J. Am. Chem. Soc.*, 2025, **147**, 1831–1839.
21 H. Li, P. Zhang, L. P. Smaga, R. A. Hoffman and J. Chan, *J. Am. Chem. Soc.*, 2015, **137**, 15628–15631.
22 F. Wang, X. Jiang, H. Xiang, N. Wang, Y. Zhang, X. Yao, P. Wang, H. Pan, L. Yu, Y. Cheng, Y. Hu, W. Lin and X. Li, *Biosens. Bioelectron.*, 2021, **172**, 112756.
23 X. Wu, L. Li, W. Shi, Q. Gong and H. Ma, *Angew. Chem., Int. Ed.*, 2016, **55**, 14728–14732.
24 J. Han, J. Li, X. Luo, G. Feng and J. Zhang, *Coord. Chem. Rev.*, 2024, **520**, 216157.
25 L. Zhang, J. C. Er, K. K. Ghosh, W. J. Chung, J. Yoo, W. Xu, W. Zhao, A. T. Phan and Y.-T. Chang, *Sci. Rep.*, 2014, **4**, 3776.
26 A. Mujeeb, M. Z. Alam, Sultan, H. Aleem Basha, S. A. Khan and S. Afzal, *J. Fluoresc.*, 2024, 1–14.
27 J. Wang, Y. Liu, X. Li, H. Lei and J. Liu, *Chem. Commun.*, 2024, **60**, 14272–14275.
28 S. Ye, H. Zhang, J. Fei, C. H. Wolstenholme and X. Zhang, *Angew. Chem., Int. Ed.*, 2020, **60**, 1339–1346.
29 J. Han, H. Ren, X. Luo, J. Li and J. Zhang, *Microchem. J.*, 2024, **207**, 111860.
30 P.-T. Chou, G.-R. Wu, C.-Y. Wei, C.-C. Cheng, C.-P. Chang and F.-T. Hung, *J. Phys. Chem. B*, 2000, **104**, 7818–7829.

